UC Berkeley

Title
Paternal chromosome loss and metabolic crisis contribute to hybrid inviability in Xenopus

Permalink
https://escholarship.org/uc/item/77v3v09f

Journal
Nature, 553(7688)

ISSN
0028-0836

Authors
Gibeaux, Romain
Acker, Rachael
Kitaoka, Maiko
et al.

Publication Date
2018

DOI
10.1038/nature25188

Peer reviewed

Paternal chromosome loss and metabolic crisis contribute to hybrid inviability in *Xenopus*

Romain Gibeaux[1], **Rachael Acker**[1], **Maiko Kitaoka**[1], **Georgios Georgiou**[2], **Ila van Kruijsbergen**[2], **Breanna Ford**[3], **Edward M. Marcotte**[5], **Daniel K. Nomura**[3], **Taejoon Kwon**[4], **Gert Jan C. Veenstra**[2], and **Rebecca Heald**[1,*]

[1]Department of Molecular and Cell Biology, University of California, CA 94720, Berkeley, USA [2]Radboud University, Department of Molecular Developmental Biology, Faculty of Science, Radboud Institute for Molecular Life Sciences, Nijmegen, The Netherlands [3]Departments of Chemistry and Nutritional Sciences and Toxicology, University of California, CA 94720, Berkeley, USA [4]Department of Biomedical Engineering, Ulsan National Institute of Science and Technology, Ulsan 44919, Korea [5]Department of Molecular Bioscience, Center for Systems and Synthetic Biology, Institute for Cellular and Molecular Biology, The University of Texas at Austin, Austin, Texas 78712, USA

Hybridization of eggs and sperm from closely related species can give rise to genetic diversity, or can lead to embryo inviability due to incompatibility. Although central to evolution, the cellular and molecular mechanisms underlying postzygotic barriers that drive reproductive isolation and speciation remain largely unknown[1,2]. Species of the African Clawed frog *Xenopus* provide an ideal system to study hybridization and genome evolution. *Xenopus laevis* is an allotetraploid with 36 chromosomes that arose through interspecific hybridization of diploid progenitors, whereas *Xenopus tropicalis* is a diploid with 20 chromosomes that diverged from a common ancestor ~48 million years ago[3]. Differences in genome size between the two species are accompanied by organism size differences, and size scaling of the egg and subcellular structures such as nuclei and spindles formed in egg extracts[4]. Nevertheless, early development transcriptional programs, gene expression patterns, and protein sequences are generally conserved[5,6]. Interestingly, whereas the hybrid produced when *X. laevis* eggs are fertilized by *X. tropicalis* sperm ($l_e \times t_s$) is viable, the reverse hybrid ($t_e \times l_s$) dies prior to gastrulation[7,8] (Fig. 1a). Here, we applied cell biological tools and high-throughput methods to study the mechanisms underlying hybrid inviability.

*Correspondence and requests for materials should be addressed to bheald@berkeley.edu.

We reveal that two specific *X. laevis* chromosomes are incompatible with the *X. tropicalis* cytoplasm and are mis-segregated during mitosis, leading to unbalanced gene expression at the maternal to zygotic transition, followed by cell-autonomous catastrophic embryo death.

Although $t_e \times l_s$ hybrid and *X. tropicalis* ($t_e \times t_s$) cleavage divisions and rate of development were very similar (Fig. 1b), hybrid embryos died abruptly as late blastulae and never initiated gastrulation. Prior to their death, hybrid embryos took on a deformed mushroom-like shape before lysing from the vegetal pole (Fig. 1c and Video 1). Explants prepared from the opposite pole (animal caps) of mid-blastula $t_e \times l_s$ embryos also died within a few hours, indicating that embryo death is cell autonomous and not a result of faulty developmental cues (Fig. 1d and Video 2). In contrast to $t_e \times l_s$ hybrids that die as embryos, haploid *Xenopus* embryos develop to the tadpole stage[8,9], suggesting that hybrid death is due to factors brought in by the *X. laevis* sperm to the *X. tropicalis* egg during fertilization. Irradiation of *X. laevis* sperm prior to fertilization, which destroys the DNA[10,11], resulted in a haploid phenotype (Fig. 1e and Videos 3, 4), indicating that $t_e \times l_s$ embryo death is due to the presence of the *X. laevis* genome. Cybrid embryos generated by irradiating *X. tropicalis* eggs, destroying the maternal DNA[8] prior to fertilization with *X. laevis* sperm, died before gastrulation similar to $t_e \times l_s$ embryos, indicating that hybrid inviability does not result from a conflict between the paternal and maternal genomes (Extended Data Table 1).

To visualize the dynamics of hybrid cell divisions, we injected mRNAs encoding fluorescent fusion proteins to label embryo chromosomes and mitotic spindles, and observed animal caps at early stage 9, which revealed anaphase defects and chromosome mis-segregation (Fig. 1f and Video 5). Immunofluorescence of whole embryos confirmed the presence of lagging chromosomes and chromosome bridges in cells throughout hybrid blastulae, as well as the formation of micronuclei in interphase, whereas no such defects were observed in *X. tropicalis* embryos (Fig. 1g) or in the reverse viable hybrid (data not shown). Imaging of $t_e \times l_s$ embryos from stage 4 (8 cells) to stage 9 (thousands of cells) revealed micronuclei in 6–10% of the cells throughout hybrid development, but not in the *X. tropicalis* control (Extended Data Fig. 1a, b), indicating that chromosome mis-segregation in $t_e \times l_s$ hybrid embryos is unrelated to changes in gene expression at the onset of zygotic genome activation (ZGA). Since the regular ploidy supported by the *X. tropicalis* egg is N=20 chromosomes, but the $t_e \times l_s$ hybrid zygote must accommodate 28 chromosomes, we tested whether an increase in ploidy was causing chromosome mis-segregation and embryo death by applying a cold shock to *X. tropicalis* zygotes a few minutes after fertilization to suppress polar body extrusion and increase their ploidy to N=30 chromosomes (Extended Data Fig. 1c). Micronuclei were not observed in cold-shocked embryos, which developed to the tailbud stage similarly to haploid embryos (Extended Data Fig. 1d). Thus, increasing the ploidy of *X. tropicalis* embryos does not cause chromosome mis-segregation or cell death, indicating a specific role for the *X. laevis* genome in hybrid inviability.

To determine whether assembly and function of the mitotic apparatus was affected, we used the *in vitro* egg extract system to examine spindle assembly and mitotic chromosome morphology. Metaphase-arrested *X. tropicalis* egg extract reconstituted spindle formation around nuclei isolated from stage 8 *X. tropicalis* (N=20), *X. laevis* (N=36), and viable hybrid embryos *(l_e×t_s*; N=28) (Fig. 2a). Spindle width scaled slightly with increasing

genome size, but microtubule distribution was not affected by either genome size or content (Extended Data Fig. 1e), indicating that the presence of *X. laevis* DNA did not impair spindle assembly in *X. tropicalis* cytoplasm. To interrogate chromosome morphology, *X. laevis* sperm nuclei were cycled through S phase in either *X. laevis* or *X. tropicalis* egg extract, induced to arrest in metaphase, and then stained with a DNA dye and antibodies to either CENP-A, the core centromeric histone variant, or Ndc80, an outer kinetochore component essential for linking centromeres to spindle microtubules[12]. Two fluorescent spots per chromosome were often visible in either extract suggesting that the *X. tropicalis* extract is capable of replicating the *X. laevis* genome to generate duplicated sister chromatids. However, we observed 13.5% fewer CENP-A-labeled and 12% fewer Ndc80-labeled chromosomes in *X. tropicalis* extract compared to *X. laevis* extract (Fig. 2b), suggesting that approximately two *X. laevis* chromosomes do not possess centromeres that become competent for kinetochore assembly following a cell cycle in *X. tropicalis* cytoplasm. Remarkably, whole genome sequencing of embryos at stage 9 prior to cell death revealed the specific loss of 228 Mb of *X. laevis* sequence from $t_e \times l_s$ hybrids (Fig. 2c), 96% of which was missing from just two chromosomes, 3L and 4L. In contrast, no genomic deletions were detected in viable $l_e \times t_s$ hybrid embryos (data not shown). Chromosome regions adjacent to breakpoints were heterogeneous in abundance (Fig. 2d), consistent with stochastic chromosome breakage and loss. Notably, major breakpoints localized to a gap in the genome assembly, indicating the presence of repetitive elements. Chromosome loss and partial deletion has been observed in nonviable hybrids in fish[13,14] and *Drosophila*[15], but the underlying mechanisms were unclear. Our results suggest that $t_e \times l_s$ hybrid incompatibility may be due to divergence of centromeric sequences, which are poorly characterized in *Xenopus* but known to evolve rapidly[16], or to other unidentified repetitive DNA elements that lead to chromosome instability and ultimately prevent kinetochore assembly on chromosomes 3L and 4L.

We next investigated the link between chromosome loss and $t_e \times l_s$ hybrid embryo death. Micronuclei in cancer cells accumulate DNA damage[17–19] and, in *Xenopus*, DNA damage was shown to trigger apoptosis at the onset of gastrulation[20]. As in cancer cells, micronuclei in $t_e \times l_s$ hybrid embryos often lost envelope integrity and contained damaged DNA (Extended Data Fig. 2a, b). However, $t_e \times l_s$ hybrid death did not resemble TUNEL-positive apoptotic death induced by chemical inhibitors of DNA replication or protein synthesis in *X. tropicalis* embryos (Extended Data Fig. 2c; Videos 6, 7; Extended Data Table 2). We hypothesized that chromosome loss could lead to cell death by affecting gene expression at ZGA. To assess the effects of blocking gene expression globally, we treated *X. tropicalis* embryos with the transcription initiation inhibitor triptolide and observed a phenotype reminiscent of the timing and manner of the catastrophic $t_e \times l_s$ hybrid embryo death, although lysis did not initiate from the vegetal side (Videos 8, 9; Extended Data Table 2). To test whether altering gene dosage could rescue hybrid viability, we applied cold shock to the hybrid zygote to suppress polar body extrusion and introduce a second copy of the *X. tropicalis* genome. Although extremely inefficient, a total of 9 triploid hybrid $tt_e \times l_s$ embryos were obtained in 4 separate experiments and survived to tailbud/tadpole stages (Fig. 3a). Rescued embryos possessed significantly higher DNA content than diploid *X. tropicalis* embryos at stage 21 (Fig. 3b), but whole genome sequencing revealed that *X. laevis* DNA

was eliminated by the tadpole stage (Extended Data Fig. 3a, Extended Data Table 3, Supplementary Table 1). Our results link $t_e \times l_s$ hybrid inviability with altered gene expression that can be rescued with a second copy of the *X. tropicalis* genome, and indicate that $t_e \times l_s$ hybrid embryo inviability is caused by defects at the onset of ZGA, and not by DNA damage and apoptosis.

Since metabolite pools are known to become crucial before gastrulation[21], we subjected $t_e \times l_s$ hybrid embryos to metabolic profiling at 7 hours post-fertilization (hpf), just prior to the characteristic deformation preceding lysis. Levels of 17 out of 179 metabolites detected were significantly altered (Fig. 3c). Reduction in lactic acid, the final product of fermentation, and tricarboxylic acid cycle intermediates revealed that glycolytic metabolism was impaired in the cytoplasm of $t_e \times l_s$ hybrid embryos, which could in turn alter lipid metabolites including neutral lipids such as diacylglycerols (DAGs) and monoacylglycerols (MAGs), as well as fatty acid oxidation metabolites such as acyl carnitines (ACs) (Extended Data Fig. 3b). While inhibition of mitochondrial ATP synthase led to cell cycle arrest at stage 9 (Video 10), perturbing the early steps of glycolysis in $t_e \times t_s$ embryos induced cell death and lysis (Video 11; Extended Data Table 2). In particular, inhibition of glycogen phosphorylase to block the release of glucose from glycogen led to cell death at stage 9, initiating from the vegetal side of the embryo (Video 12). These results are consistent with glycolytic defects as a primary cause of $t_e \times l_s$ hybrid embryo death. However, other defects that contribute to hybrid incompatibility could be masked by the abrupt cell lysis, such as conflicts between the paternal genome and maternal mitochondria[22,23].

To evaluate the link between the metabolic defects and specific chromosome loss, we used a statistical analysis[24] to classify the list of 1803 genes mapped to the regions lost from chromosomes 3L and 4L in $t_e \times l_s$. We found that metabolic processes, particularly in glycolysis, were significantly over-represented (Extended Data Table 4). Transcriptome profiling of $t_e \times l_s$ hybrid embryos at 7 hpf (Supplementary Table 2) revealed that although a large fraction of genes lost from chromosomes 3L and 4L were not differentially expressed compared to wild type embryos (>92%; Fig. 3d), 27.1% of the differentially expressed genes related to metabolism (Fig. 3e; top), including PDK1 (pyruvate dehydrogenase kinase). Moreover, 36.7% of the significantly under-expressed metabolism genes are found on chromosomes 3L and 4L (Fig. 3e; bottom), including GFPT1 (fructose-6-phosphate aminotransferase) and HPDL (4-hydroxyphenylpyruvate dioxygenase).

To further characterize the specificity and mechanism underlying $t_e \times l_s$ hybrid incompatibility, we compared the outcome of cross-fertilizations between *X. tropicalis* and another allotetraploid *Xenopus* species, *X. borealis*[25]. Analogous to hybridization between *X. laevis* and *X. tropicalis*, we observed that *X. borealis* eggs fertilized with *X. tropicalis* sperm ($b_e \times t_s$) were viable while the reverse hybrid ($t_e \times b_s$) was not (Fig. 4a). However, the $t_e \times b_s$ embryos did not lyse, but exogastrulated and survived for hours with intact cells (Fig. 4b–c; Video 13). Similar to $t_e \times l_s$, $t_e \times b_s$ embryos displayed chromosome loss through anaphase defects and formation of micronuclei (Fig. 4d, Extended Data Fig. 4a–c). Strikingly, whole $t_e \times b_s$ hybrid genome sequencing revealed that, although the loss was specific for the paternal genome as in the $t_e \times l_s$ hybrid, specific regions of four different *X. borealis* chromosomes were affected (Fig. 4e–f, Extended Data Table 3, Supplementary

Table 1). Furthermore, metabolomics of $t_e \times b_s$ embryos revealed a distinct profile with less severe alterations than observed for $t_e \times l_s$ (Fig. 4g).

Altogether, our results indicate that hybrid instability in *Xenopus* results primarily from post-zygotic conflicts between the maternal cytoplasm and the paternal genome that lead to loss of specific genomic regions and downstream gene dosage defects. These findings highlight the role of genome evolution and transmission in defining hybrid fates and speciation.

METHODS

Chemicals

Unless otherwise stated, all chemicals were purchased from Sigma-Aldrich, St. Louis, MO.

Frogs

All animal experimentation is this study was performed according to our Animal Use Protocol approved by the UC Berkeley Animal Care and Use Committee. Mature *X. laevis*, *X. tropicalis*, and *X. borealis* frogs were obtained from NASCO, WI, or the National *Xenopus* Resource (NXR, Woods Hole, MA). Female *X. laevis* (1 to 4 years old), *X. tropicalis* (6 months to 4 years old), and *X. borealis* (from 2 to 3 years old) frogs were ovulated with no harm to the animals with 6-, 3-, and 4-month rest intervals, respectively. To obtain testes, males (same age ranges) were euthanized by over-anaesthesia through immersion in ddH$_2$O containing 0.15% MS222 (Tricaine) neutralized with 5 mM sodium bicarbonate prior to dissection, and then frozen at −20°C.

Experimental design

Sample sizes were not pre-specified and were sufficient to generate statistically significant differences. All attempts at replication where successful. All experiments were performed independently at least 3 times (biological replicates). *Xenopus* frogs were selected randomly from our colony for ovulation and fertilization experiments. Investigators were not blinded.

In vitro fertilization and cross-fertilization

X. laevis males were injected with 500 U of human chorionic gonadotropin hormone (hCG) 12–24 h before dissection and testes were stored at 4°C in 1X MR (100 mM NaCl, 1.8 mM KCl, 2 mM CaCl$_2$, 1 mM MgCl$_2$ and 5 mM HEPES-NaOH pH 7.6) for 1–2 weeks. *X. tropicalis* and *X. borealis* males were injected with 250 U and 300 U, respectively, of hCG 12–24 h before dissection and testes were collected in Leibovitz L-15 Medium (Gibco – Thermo Fisher Scientific, Waltham, MA) supplemented with 10% Fetal Bovine Serum (FBS; Gibco) for immediate use.

For *X. tropicalis* egg-based embryos, *X. tropicalis* females were primed with 25 U of hCG 12–24 h before use and boosted with 250 U of hCG on the day of the experiment. As soon as the first eggs were laid (~3 h after boosting), the *X. tropicalis* male was euthanized and dissected. Two *X. tropicalis* or *X. borealis* testes, or 1/3 of a *X. laevis* testis were each added to 1 mL of L-15 10% FBS. *X. tropicalis* females were squeezed gently to deposit eggs onto

petri dishes coated with 1.5% agarose in 1/10X MMR (1X MMR: 100 mM NaCl, 2 mM KCl, 2 mM $CaCl_2$, 1 mM $MgSO_4$ and 5 mM HEPES-NaOH pH 7.6, 0.1 mM EDTA). Testes were homogenized using scissors and a pestle in L-15 10% FBS. Any liquid in the petri dishes was removed and the eggs were fertilized with 500 μL of sperm solution per dish. Eggs were swirled in the solution to separate them and incubated for 4 min with the dish slanted. Dishes were then flooded with ddH_2O, swirled and incubated for 5–10 min. Buffer was exchanged for 1/10X MMR, the eggs incubated for 10 min and jelly coats removed with a 3% cysteine solution (in ddH_2O-NaOH, pH 7.8). After extensive washing with 1/10X MMR (>4X), embryos were incubated at 23°C. At stage 2–3, fertilized embryos were sorted and placed in fresh 1/10X MMR within new petri dishes coated with 1.5% agarose in 1/10X MMR.

For *X. laevis* egg-based embryos, *X. laevis* females were primed with 100 U of pregnant mare serum gonadotropin (PMSG, National Hormone and Peptide Program, Torrance, CA) at least 48 h before use and boosted with 500 U of hCG 14 hours before the experiment. *X. laevis* females were squeezed gently to deposit eggs onto petri dishes coated with 1.5% agarose in 1/10X MMR. Two *X. tropicalis* testes collected in L-15 10% FBS or 1/3 of a *X. laevis* testes were each added to 1 mL of ddH_2O and homogenized using scissors and a pestle. Any liquid in the petri dishes was removed and the eggs were fertilized with 500 μL of sperm solution per dish. Eggs were swirled in the solution to individualize eggs as much as possible and incubated for 10 min. Dishes were flooded with 1/10X MMR, swirled and incubated for 10–20 min. Jelly coats were removed with a 2% cysteine solution (in ddH_2O-NaOH, pH 7.8). After extensive washing (>4X) with 1/10X MMR, embryos were incubated at 23°C. At stage 2–3, fertilized embryos were sorted and placed in fresh 1/10X MMR in new petri dishes coated with 1.5% agarose in 1/10X MMR.

For *X. borealis* egg-based embryos, *X. borealis* females were primed with 60 U of PMSG at least 48 hours before use and boosted with 300 U of hCG 14 h before the experiment. Frogs were kept at 16°C in 1/2X MMR. Eggs were picked from the tub and deposited onto petri dishes coated with 1.5% agarose in 1/10X MMR. Two *X. tropicalis* or *X. borealis* testes were collected and homogenized using scissors and a pestle in L-15 10% FBS. Any liquid in the petri dishes was removed and the eggs were fertilized with 500 μL of sperm solution per dish. Eggs were swirled in the solution to individualize eggs as much as possible and incubated for 10 min. Dishes were flooded with 1/10X MMR, swirled and incubated for 10–20 min. Jelly coats were then removed with a 3% cysteine solution (in ddH_2O-NaOH, pH 7.8). After extensive washing (>4X) with 1/10X MMR, embryos were incubated at 23°C. At stage 2–3, fertilized embryos were sorted and placed in fresh 1/10X MMR in new petri dishes coated with 1.5% agarose in 1/10X MMR.

All embryos were staged according to Nieuwkoop and Faber[26].

Embryo chemical treatments and video imaging

Chemical treatments were performed in petri dishes coated with exactly 5 mL of 1.5% agarose in 1/10X MMR covered with 10 mL 1/10X MMR for either regular incubations or video imaging for consistency. Concentrations were calculated relative to the covering volume of 1/10X MMR, no dilution within the volume in the agarose was assumed.

Cycloheximide was added at a concentration of 0.1 mg/mL at stage 6.5 from 8 mg/mL stock in DMSO. Hydroxyurea (Thermo Fisher Scientific, Waltham, MA) was added at a concentration of 30 mM at stage 3 from 600 mM stock in ddH$_2$O. Triptolide was added at a concentration of 25 μM at stage 2 from 25 mM stock in DMSO. Oligomycin was added at a concentration of 40 μM at stage 2 from 40 mM stock in DMSO. AP-III-a4 was added at a concentration of 30 μM at stage 2 from 1 mM stock in DMSO. Iodoacetic acid was added at a concentration of 50 mM at stage 2 from 1 M stock in ddH$_2$O. CP-91,149 was added at a concentration of 270 μM at stage 2 from 30 mM stock in DMSO. Corresponding volumes of DMSO or ddH$_2$O were added to controls.

Imaging dishes were prepared using a homemade PDMS mold designed to print a pattern of 0.9 mm large wells in agarose that allowed us to image 6 *X. tropicalis* embryos simultaneously within the 3X4 mm camera field of view for each condition. Embryos were imaged from stage 2–3. Treatment and control videos were taken simultaneously using two AmScope MD200 USB cameras (AmScope, Irvine, CA) each mounted on an AmScope SE305R stereoscope. Time lapse movies were acquired at a frequency of 1 frame every 10 s for 20 h and saved as Motion JPEG using a MATLAB (The MathWorks, Inc., Natick, MA) script. Movie post-processing (cropping, concatenation, resizing, addition of scale bar) was done using MATLAB and Fiji[27]. All MATLAB scripts written for this study are available upon request. Two of the scripts used here were obtained through the MATLAB Central File Exchange: "videoMultiCrop" and "concatVideo2D" by Nikolay S.

Embryo ploidy manipulations

To generate *X. tropicalis* haploid embryos ($t_e \times [t_s]$ and $t_e \times [l_s]$), fertilizations were conducted as detailed above with slight modifications to accommodate for sperm UV-irradiation. Two *X. tropicalis* testes or 1/3 of a *X. laevis* testis were each added to 1.1 mL of L-15 10% FBS. Testes were homogenized using scissors and a pestle and the solutions spun briefly using a benchtop centrifuge to pellet the tissue. 1 mL of supernatant was transferred into a glass petri dish and irradiated within a Stratalinker UV-Crosslinker (Stratagene, San Diego, CA) with 50,000 microjoules for *X. tropicalis* sperm or 2 times 30,000 microjoules for *X. laevis* sperm, swirling the solution in between the two irradiations. *X. tropicalis* eggs freshly squeezed onto petri dishes coated with 1.5% agarose in 1/10X MMR were then fertilized with 500 μL of irradiated sperm solution per dish and processed as described above.

To generate $[t_e] \times l_s$ cybrid embryos and the haploid $[t_e] \times t_s$ controls, fertilizations were conducted as detailed above with slight modifications to accommodate for the UV-irradiation of the eggs. Two *X. tropicalis* testes or 2/3 of a *X. laevis* testis were each added to 1.1 mL of L-15 10% FBS. *X. tropicalis* females were squeezed gently to deposit eggs onto petri dishes coated with 1.5% agarose in 1/10X MMR. Excess liquid was removed, eggs were swirled with a pestle to form a monolayer of properly oriented eggs and immediately irradiated within a Stratalinker UV-Crosslinker (Stratagene, San Diego, CA) 2 times with 40,000 microjoules. Testes were homogenized using scissors and a pestle during the irradiation of the eggs. As soon as irradiated, the eggs were fertilized with 500 μL of sperm solution per dish and processed as described above.

To prevent polar body formation in either $tt_e \times t_s$ or $tt_e \times l_s$ experiments, fertilizations were conducted as detailed above with slight modifications to accommodate cold treatment. Fertilizations were performed within dishes coated with only 1–1.5 mL, instead of 5 mL, of 1.5% agarose in 1/10X MMR to accelerate cooling. Following the 4-min incubation with sperm, dishes were flooded with ddH$_2$O, swirled and incubated for exactly 5 min. Buffer was then exchanged for ice-cold 1/10X MMR, the dishes transferred into a pipette tip box lid placed in a slushy ice bucket, and the eggs were incubated for 10 min. The dishes were then removed from the bucket and the cold buffer was exchanged for RT 1/10X MMR. After 20 min, the jelly coat was removed with a 3% cysteine solution (in ddH$_2$O-NaOH, pH 7.8) and the embryos processed as described above.

Animal cap assay

At stage 8, embryos were placed in Danilchik's for Amy Medium (DFA medium; 53 mM NaCl, 5 mM Na$_2$CO$_3$, 4.5 mM Potassium gluconate, 32 mM Sodium gluconate, 1 mM CaCl$_2$, 1 mM MgSO$_4$, pH 8.3, 1 g/L BSA and 0.8% Antibiotic Antimycotic Solution) for surgery. Using Dumostar-Biology 55 forceps (Dumont, Montignez, Switzerland), the vitelline membrane was removed and the animal cap was isolated from the embryo. The caps were finally transferred to a new dish or a chamber containing fresh DFA medium for imaging.

mRNA, embryo microinjection, and animal cap confocal microscopy

Plasmids for expression of EB3-GFP and histone H2B-RFP mRNAs were obtained at the 2013 Advanced Imaging in *Xenopus* Workshop from the Wallingford lab (UT Austin, USA). The mRNAs were synthetized using mMessage mMachine SP6 Transcription Kit (Ambion – Thermo Fisher Scientific, Waltham, MA) following supplier protocol. The mRNAs were purified using Phenol-Chloroform extraction, resuspended in ddH$_2$O, aliquoted and stored at −80°C.

At stage 2, $t_e \times l_s$ hybrid embryos were transferred to 1/9X MMR 3% Ficoll. A solution containing 50 pg/nL of H2B-RFP mRNA and 100 pg/nL of EB3-GFP mRNA, concentrations which allowed us to image fluorescent signal as early as stage 9, was loaded into a needle pulled from 1 mm glass capillary tube (TW100F-4, World Precision Instruments, Inc., Sarasota, FL) using a P-87 Micropipette Puller (Sutter Instrument, Navato, CA). Embryos were placed in a mesh-bottomed dish and microinjected in both blastomeres with 1 nL of the mRNA solution using a Picospritzer III microinjection system (Parker, Hollis, NH) equipped with a MM-3 micromanipulator (Narishige, Amityville, NY). Injected embryos were transferred to a new dish and incubated at 23°C in 1/9X MMR 3% Ficoll until stage 8 when they were processed for animal cap isolation as described above. Caps were placed in a chamber filled with DFA medium made using 1×1 cm Gene Frames (Thermo Fisher Scientific, Waltham, MA) between a slide and a coverslip (Thermo Fisher Scientific, Waltham, MA) for confocal microscopy.

Embryo whole mount immunofluorescence

At desired stages, embryos were fixed for 1–3 h using either MAD fixative (2 parts of methanol (Thermo Fisher Scientific, Waltham, MA), 2 parts of acetone (Thermo Fisher

Scientific, Waltham, MA), 1 part of DMSO) for most antibodies or MEMFA fixative (0.1 M MOPS pH 7.4, 2 mM EGTA, 1 mM $MgSO_4$, 3.7% formaldehyde) for the γH2A.X antibody. After fixation, embryos were dehydrated in methanol and stored at −20°C. Embryos were then processed as previously described[28] with some modifications. Following gradual rehydration in 0.5X SSC (1X SSC: 150 mM NaCl, 15 mM Na citrate, pH 7.0), embryos were bleached with 1–2% H_2O_2 (Thermo Fisher Scientific, Waltham, MA) in 0.5X SSC containing 5% formamide for 2–3 h under light, then washed in PBT, a PBS solution containing 0.1% Triton X-100 (Thermo Fisher Scientific, Waltham, MA) and 2 mg/mL bovine serum albumin (BSA). Embryos were blocked in PBT supplemented with 10% goat serum (Gibco – Thermo Fisher Scientific, Waltham, MA) and 5% DMSO for 1–3 h and incubated overnight at 4°C in PBT supplemented with 10% goat serum and the primary antibodies. We used different combinations of the following antibodies: 1:500 mouse anti-beta tubulin (E7; Developmental Studies Hybridoma Bank, Iowa City, IA), 1:500 rabbit anti-histone H3 (ab1791; Abcam, Cambridge, MA), 1:500 rabbit anti-lamin B1 (ab16048; Abcam, Cambridge, MA), 1:500 mouse anti-phospho-histone H2A.X (05-636; EMD Millipore, Merck KGaA, Darmstadt, Germany). Embryos were then washed 4 X 2 h in PBT and incubated overnight in PBT supplemented with 1:500 goat anti-mouse or goat anti-rabbit secondary andibodies coupled either to Alexa Fluor 488 or 568 (Invitrogen – Thermo Fisher Scientific, Waltham, MA) and with 1:200 YO-PRO iodide (Thermo Fisher Scientific, Waltham, MA) if the use of anti-histone H3 antibody as primary was not possible. Embryos were then washed 4 X 2 h in PBT and gradually dehydrated in methanol. Embryos were finally cleared in Murray's clearing medium (2 parts of Benzyl Benzoate, 1 part of Benzyl Alcohol). Embryos were placed either in a chamber made using a flat nylon washer (Grainger, Lake Forest, IL) attached with nail polish (Sally Hansen, New York, NY) to a slide and covered by a coverslip or a chamber made of silicon grease (Beckman coulter, Brea, CA) between slide and coverslip, and filled with Murray's clearing medium for confocal microscopy.

Confocal microscopy, micronuclei and nuclear size quantification

Confocal microscopy was performed on a Zeiss LSM 780 NLO AxioExaminer using the Zeiss Zen Software. For animal cap live imaging, histone H2B-RFP and EB3-GFP signals were imaged on a single plane with a frame size of 1024×1024 px every 5 s using a Plan-Apochromat 40x/1.4 Oil objective and laser power of 22%. For imaging of histone H3, embryos were imaged using a Plan-Apochromat 20x/1.0 Water objective and laser power of 12%, on multiple 1024×1024 px plans spaced of 0.68 μm in Z. For characterization of the micronuclei (lamin B1 and γH2A-X), embryos were imaged using a Plan-Apochromat 63x/1.40 Oil objective and laser power of 12%, on multiple plans spaced 0.38 μm in Z. Images are mean averages of 2 scans with a depth of 16 Bits. Pinhole size was always chosen to correspond to 1 airy unit.

Micronuclei were quantified at stages 4, 6, 7, 8 and 9 as the number of observed micronuclei in the dataset divided by the number of nuclei in the dataset. The number of micronuclei at all stages and of nuclei at stage 4 and 6 were counted manually in Fiji. The number of nuclei at stages 7, 8 and 9 was determined automatically through histone H3 fluorescence signal segmentation using Imaris (Bitplane, Zurich, Switzerland). Nuclear area in $tt_e \times t_s$, X.

tropicalis and $t_e \times [t_s]$ was measured in Fiji using the ellipse tool. From this, we calculated the diameter of a circle of the same area, a value that we could directly compare the cell size determined through the measurement of the cell diameter at the nucleus central plan.

Embryo nuclei purification

Embryo nuclei were prepared as previously described[29] from *X. tropicalis*, $l_e \times t_s$ hybrid, and *X. laevis* embryos. Briefly, embryos were arrested at stage 8 in late interphase using 150 μg/mL cycloheximide in 1/10X MMR for 60 min. Then they were washed several times in ELB (250 mM sucrose, 50 mM KCl, 2.5 mM $MgCl_2$, and 10 mM HEPES pH 7.8) supplemented with LPC (10 μg/mL each leupeptin, pepstatin, chymostatin), cytochalasin D (100 μg/mL), and cycloheximide (100 μg/mL), packed in a tabletop centrifuge at 200 g for 1 min, crushed with a pestle, and centrifuged at 10,000 g for 10 min at 16°C. The cytoplasmic extract containing endogenous embryonic nuclei was collected, supplemented with 8% glycerol, aliquoted, frozen in liquid nitrogen and stored at −80°C.

Xenopus egg extracts and related methods

X. laevis[30] and *X. tropicalis*[4] metaphase arrested egg extracts were prepared and spindle reactions conducted as previously described.

To reconstitute spindle assembly, stage 8 embryo nuclei were used as a source of DNA. Aliquots were thawed, resuspended in 1 mL of ELB, and spun at 1600 g for 5 min at RT. Pelleted nuclei were resuspended in 25 μL of fresh *X. tropicalis* extract and incubated at RT. To examine kinetochore assembly, *X. laevis* sperm nuclei, prepared as previously described[31], were used as a source of DNA in both *X. laevis* and *X. tropicalis* egg extracts. Cycled chromosomes were prepared and spun-down[30] and then processed for immunofluorescence as previously described[32]. Briefly, the coverslips were incubated for 1 min in cold methanol, washed with PBS+NP40 and blocked overnight in PBS + 5% BSA at 4°C. The anti-Ndc80 (1:300 dilution, Stukenberg lab, University of Virginia) or the anti-CENP-A (1:500 dilution, Straight lab, Stanford University) rabbit antibodies were added for 1 h. After washing with PBS+NP40, the coverslips were incubated with 1:1000 anti-rabbit antibody coupled to Alexa Fluor 488 (Invitrogen – Thermo Fisher Scientific, Waltham, MA) for 30 min and then with 1:1000 Hoechst for 5 min. The coverslips were finally washed and mounted for imaging. Each presented dataset was obtained from 3 different egg extracts with technical duplicates for each. Spindles and chromosomes were imaged using micromanager software[33] with an Olympus BX51 microscope equipped with an ORCA-ER or an ORCA-II camera (Hamamatsu Photonics, Hamamatsu city, Japan), and with an Olympus UPlan FL 40X air objective. Spindle measurements were made using Fiji and the spindle tubulin intensity line scan using an automated Java ImageJ plugin developed by Xiao Zhou (Heald lab, UC Berkeley; https://github.com/XiaoMutt/AiSpindle).

TUNEL assay

Embryos were fixed in MEMFA as described for embryo whole mount immunofluorescence and processed as previously described[20] with minor modifications. Briefly, after gradual rehydration, embryos were bleached with 1–2% H_2O_2 in 0.5X SSC containing 5% formamide for 1–2 h under light. After washes in PBS, embryos were incubated in 1X

Terminal Deoxynucleotidyl Transferase (TdT) Buffer for 1 h and then overnight in TdT Buffer supplemented with 150 U/ml of TdT enzyme (Invitrogen – Thermo Fisher Scientific, Waltham, MA) and 1 pmol/μL Digoxigenin-11-dUTP (Roche, Basel, Switzerland). After washes in 1 mM EDTA/PBS at 65°C, in PBS and then in MAB (100 mM maleic acid, 150 mM NaCl, pH 7.5), embryos were blocked for 1 h in 2% Blocking Reagent (Roche, Basel, Switzerland) in MAB and then incubated overnight at 4°C in 2% Blocking Reagent in MAB supplemented with 1:3000 anti-Digoxigenin AP antibody (Roche, Basel, Switzerland). After washes in MAB and in AP Buffer (100 mM Tris, pH 9.5, 50 mM MgCl$_2$, 100 mM NaCl, 0.1% Tween 20, 2 mM Levamisol), embryos were stained with NBT/BCIP (nitro-blue tetrazolium/5-Bromo-4-chloro-3-indolyl phosphate; Promega, Sunnyvale, USA) diluted in AP buffer. Reactions were stopped in MAB and embryos fixed overnight in Bouin's solution. After washes in 70% buffered ethanol and in methanol, embryos were imaged in methanol with the ToupView software (ToupTek, Zhejiang, China) using an AmScope MD200 USB camera mounted on M5 stereoscope (Wild Heerbrugg, Gais, Switzerland).

Nucleic acid isolation, library construction, and sequencing

For genomic DNA, embryos at desired stages were incubated overnight in lysis buffer (50 mM Tris-HCl, 5 mM EDTA, 100 mM NaCl, 0.5% SDS) containing 250 μg/mL Proteinase K (Roche, Basel, Switzerland). DNA was isolated using Phenol-Chloroform extraction and ethanol precipitation. To isolate RNAs, embryos at desired stages were homogenize mechanically in TRIzol® (Thermo Fisher Scientific, Waltham, MA) using up to a 30-gauge needle and processed according to supplier instructions. After resuspension in nuclease-free H2O, RNAs were cleaned up using RNeasy kit (Qiagen Inc.) with on-column DNA digestion, following supplier protocol.

Libraries were constructed at the Functional Genomics Lab (FGL), a QB3-Berkeley Core Research Facility at UC Berkeley. For genomic DNA, an S220 Focused-Ultrasonicator (Covaris®) was used to fragment DNA. The fragmented DNA was cleaned and concentrated with the MinElute® PCR Purification kit (Qiagen Inc.). The Library preparation was done on an Apollo 324™ with PrepX™ ILM 32i DNA Library Kits (WaferGen Biosystems, Fremont, CA), and 7 cycles of PCR amplification was used for library fragment enrichment. For RNAs, mRNA enrichment was performed on total RNA using polyA selection with the Invitrogen Dynabeads mRNA Direct kit. The library preparation was done on the Apollo324™ with PrepX™ RNAseq Library Prep Kits (WaferGen Biosystems, Fremont, CA), and 13 cycles of PCR amplification was used for index addition and library fragment enrichment.

Sequencing was performed by the Vincent J. Coates Genomics Sequencing Laboratory at UC Berkeley. All samples have been run as 100 paired-end HiSeq4000 lanes, pooled equimolar after quantification using KAPA Illumina Library quantification qPCR reagents on the BioRad CFX connect. Demultiplexing was performed to allow a single mismatch with Illumina's bcl2fastq version 2.17 software.

Genomic DNA sequencing analysis and deletion detection in hybrids

DNA sequencing reads were mapped to a *X. laevis - X. tropicalis* hybrid genome (Xenla9.1 and Xentro9.0) or a *X. borealis - X. tropicalis* hybrid genome (Xbo_04Apr2017 (Mudd and Rokhsar, unpublished) and Xentro9.0) using bwa mem (version 0.7.10-r789) with default settings. Duplicate reads were marked using bamUtil v1.0.2.

Deletions in $t_e \times l_s$ and $l_e \times t_s$ hybrids were called by comparing local DNA sequencing read coverage between hybrid ($t_e \times l_s$ or $l_e \times t_s$) and parental ($t_e \times t_s$ or $l_e \times l_s$) genomes. The read coverage was determined in 10kb regions, with a 2kb sliding window across the genome. For each 10kb region we calculated the RPKM in $t_e \times l_s$, $l_e \times t_s$, $t_e \times t_s$ and $l_e \times l_s$ sequencing tracks. The ratio of median RPKM values in retained regions has a non-zero baseline as expected because of a different size of hybrid and parental genomes. The ratio cut-off for deleted regions was set accordingly at 4-fold and 6-fold for *X. laevis* and *X. tropicalis* sequences, respectively. Lost regions overlapping for more than 30% of their length with gaps were removed and regions within 10kb of each other were merged. Lost genes were analyzed using the PANTHER database[24]. Because PANTHER only provided adjusted p-values for fold enrichment based on binomial test, we additionally estimated the 95% confidence interval for each enriched pathways using binom.test() function in R (version 3.2.2).

Deletions in $t_e \times b_s$ hybrids were called by identifying reduced genomic DNA signal in $t_e \times b_s$. The RPKM read coverage was determined in 10kb regions, with a 2kb sliding window across the genome. Regions with median log10 RPKM less than -1.25 in the *X. tropicalis* genome and -1.15 in the *X. borealis* genome were marked as deleted. Lost regions overlapping for more than 30% of their length with gaps were removed and regions within 10kb of each other were merged.

RNA sequencing analysis

We mapped RNA-seq reads to the combined primary transcripts of *X. laevis* (JGIv18pV4) and *X. tropicalis* (JGIv91) using bwa mem (version 0.7.10), and discarded all reads mapped in multiple targets for further analysis. To use human gene annotation, which is more comprehensive than *Xenopus*, we transferred the expression level of these species to human orthologs. Based on the best BLASTP hit to human longest protein sequences (from EnsEMBL version 80), we merged the read counts of *X. laevis* and *X. tropicalis* genes to corresponding human genes, then performed differential expression analysis with EdgeR[34]. An adjusted P-value criterion of less than 0.05 was applied to determine the significance of differential expression. To estimate the 95% confidence interval of log-scale fold change, we used limma[35] (version 3.28.10). Results of both EdgeR and Limma analyses are presented in Supplementary Table 2. For metabolic gene analysis, we used the list of metabolic genes obtained from the PANTHER database[24].

Metabolomic profiling

Seven hours post-fertilization, $t_e \times l_s$ hybrid, $t_e \times b_s$ hybrid, and respective *X. tropicalis* control embryos were collected from 3 independent fertilizations, always using eggs from the same female between the $t_e \times l_s$ hybrid or the $t_e \times b_s$ hybrid, and its *X. tropicalis* control. Five

samples of 8 embryos each for nonpolar lipid metabolites and 12 embryos each for polar metabolites were rinsed twice in filtered PBS and frozen in liquid nitrogen. Nonpolar lipid metabolites from the 8 embryos were extracted in 3 mL of 2:1 chloroform:methanol and 1 mL of PBS with inclusion of internal standards C12 monoalkylglycerol ether (MAGE) (10 nmol, Santa Cruz Biotechnology) and pentadecanoic acid (10 nmol). Organic and aqueous layers were separated by centrifugation at 1000 g for 5 min and the organic layer was collected, dried under a stream of nitrogen and dissolved in 120 μl chloroform. Polar metabolites were extracted from the 12 embryos in 180 μL of 40:40:20 (ACN:MeOH:H_2O) with inclusion of internal standard D3N15 serine (50 nM, Cambridge Isotope Laboratories, Inc. #DNLM-6863). Samples were disrupted by sonication then centrifuged at 21,000 g for 10 min and the supernatant was collected for analysis. Metabolites were separated by liquid chromatography and MS analysis was performed with an electrospray ionization (ESI) source on an Agilent 6430 QQQ LC-MS/MS (Agilent Technologies). The capillary voltage was set to 3.0 kV, and the fragmentor voltage was set to 100 V. The drying gas temperature was 350°C, the drying gas flow rate was 10 l/min, and the nebulizer pressure was 35 psi. Metabolites were identified by single reaction monitoring (SRM) of the transition from precursor to product ions at associated optimized collision energies and retention times as previously described[36]. Metabolites were quantified by integrating the area under the curve, then normalized to internal standard values and tissue weight. Metabolite levels are expressed as relative abundances as compared to controls. P-values were calculated using a two-tailed homoscedastic t-test. Significance was analyzed for an $\alpha = 0.05$ threshold as well as that with a Bonferroni-like correction to account for multiple hypothesis comparison. Strict Bonferroni correction is highly conservative and often results in increased type II errors (failing to acknowledge a real effect) and several alternatives exist. Because we compared around 200 compounds between two types of embryos, each with 5 replicates, we used a penalized Bonferroni correction, and divided the α threshold value by the logarithm of the number of tests ($\alpha/\log(k)$) to decrease the risk for the type II error.

Data availability

All genomic and transcriptomic data generated for this study are available from public databases: stage 9 $t_e \times l_s$ hybrid whole genome sequencing data (NCBI SRA: SRP124316; https://www.ncbi.nlm.nih.gov/Traces/study/?acc=SRP124316) and corresponding stage 9 *X. laevis, X. tropicalis* and $l_e \times t_s$ hybrid controls (NCBI GEO: GSE92382; https://www.ncbi.nlm.nih.gov/geo/query/acc.cgi?acc=GSE92382), tailbud and tadpole stage $tt_e \times l_s$ hybrid whole genome sequencing data (NCBI SRA: SRP124316; https://www.ncbi.nlm.nih.gov/Traces/study/?acc=SRP124316), stage 9 $t_e \times b_s$ hybrid whole genome sequencing data (NCBI SRA: SRP124316; https://www.ncbi.nlm.nih.gov/Traces/study/?acc=SRP124316) and 7 hpf *X. tropicalis* and $t_e \times l_s$ hybrid transcriptome RNA-seq data (NCBI GEO: GSE106157; https://www.ncbi.nlm.nih.gov/geo/query/acc.cgi?acc=GSE106157).

Code availability

MATLAB scripts were written to acquire and process embryo live imaging movies. All these scripts are available from the corresponding author upon request. Two MATLAB scripts used here for movie cropping and concatenation were obtained through the MATLAB

Central File Exchange: "videoMultiCrop" and "concatVideo2D" by Nikolay S. The automated spindle tubulin intensity line scan Java ImageJ plugin developed by Xiao Zhou (Heald lab, UC Berkeley) is available on GitHub (https://github.com/XiaoMutt/AiSpindle).
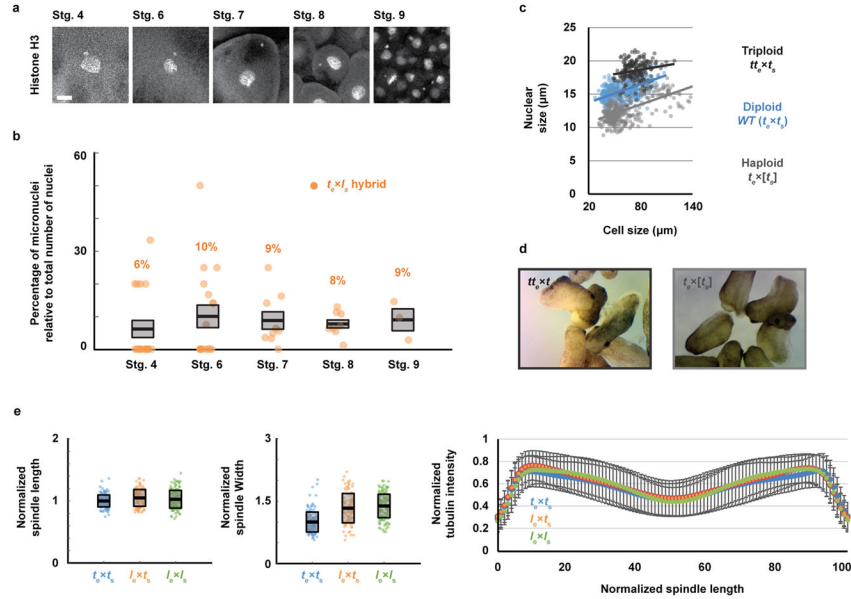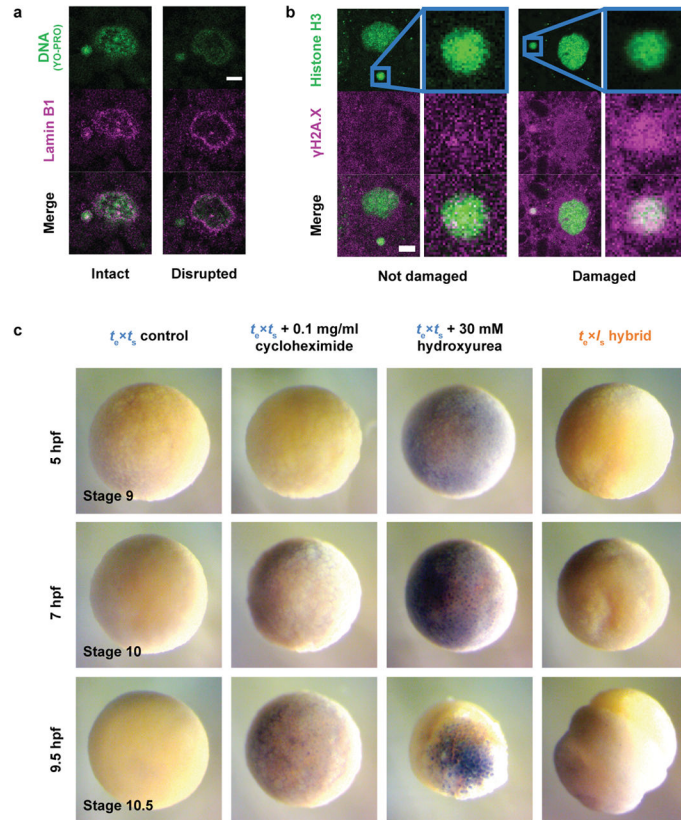
Extended Data

Extended Data Figure 1. Occurrence of micronuclei, role of ploidy and spindle architecture
a, Micronuclei in $t_e \times l_s$ hybrid embryos at various developmental stages. Whole mount embryo immunofluorescence was performed in $t_e \times l_s$ hybrid embryos using anti-histone H3 antibody at stages 4, 6, 7, 8 and 9 and quantified in b. Scale bar is 10 μm. **b,** Quantification of micronuclei in $t_e \times l_s$ hybrid embryos. The percentage of micronuclei was calculated as the number of micronuclei in the imaged portion of the embryo divided by the total number of nuclei in the same imaged portion. The average percentage for multiple embryos at stage 4 (n = 18 $t_e \times l_s$ hybrid embryos (individual dots) with a total of 63 nuclei), stage 6 (n = 17/115), stage 7 (n = 9/322), stage 8 (n = 8/1119) and stage 9 (n = 3/2004) from 3 independent experiments, is shown as thick line. Gray boxes indicate a 1 standard error of the mean. Control *X. tropicalis* embryos from the same mothers were analyzed but no micronuclei were observed at any stages. **c,** Nuclear size in *X. tropicalis* embryos with varying ploidy. Nuclear size relative to cell size (diameters in μm) is plotted for triploid ($tt_e \times t_s$; dark grey, n = 175 nuclei from 6 embryos), diploid (*X. tropicalis*, $t_e \times t_s$; blue, n = 453/9) and haploid ($t_e \times [t_s]$; light grey, n = 346/16) embryos. Each dot indicates an individual data point and the solid lines indicate a linear fit. **d,** *X. tropicalis* embryos with varying ploidy at tailbud stage. Images of triploid ($tt_e \times t_s$; left) and haploid ($t_e \times [t_s]$; right) tailbuds were taken under identical conditions. Similar observations were over 3 independent experiments. **e,** Size and microtubule distribution in *X. tropicalis* spindles assembled from different embryo nuclei DNA (n = 147, 103, and 156 spindles quantified for *X. tropicalis*, $l_e \times t_s$ hybrids, and *X. laevis* embryo nuclei, respectively, from 3 different egg extracts). Spindle length (left) and width (middle) were normalized to the *X. tropicalis* control, averages are shown as thick black lines and the gray boxes indicate 1 standard deviation.

95% confidence intervals for lengths are 1±0.02 for $t_e \times t_s$, 1.05±0.03 for $l_e \times t_s$, and 1.03±0.02 for $l_e \times l_s$ and for widths are 1±0.04, 1.3±0.07, and 1.4±0.04. Line scans of rhodamine-tubulin signal along spindle length were taken (right). Spindle lengths were normalized to 100% and tubulin intensities were normalized within datasets. The average intensities are plotted for the three spindle types, error bars indicate standard deviation and colors are as in Figure 2a.


Extended Data Figure 2. Characterization of micronuclei in $t_e \times l_s$ hybrid embryos and link to embryo death

a, Disrupted micronuclei envelopes in $t_e \times l_s$ hybrid embryos. Whole mount embryo immunofluorescence was performed in $t_e \times l_s$ hybrid embryos using the YO-PRO DNA dye (top) and anti-Lamin B1 antibody (middle), corresponding channels are shown in green and magenta, respectively. The merged images are shown below. 25 micronuclei within 5 different embryos were analyzed. Intact (left) and disrupted (right) envelopes were observed in all analyzed embryos. Scale bar is 10 μm. **b,** DNA damage in $t_e \times l_s$ hybrid embryo micronuclei. Whole mount embryo immunofluorescence was performed in $t_e \times l_s$ hybrid embryos using anti-histone H3 (top) and anti-γH2A.X (middle) antibodies, corresponding channels are shown in green and magenta, respectively. The merge images are shown below. 21 micronuclei within different 6 embryos were analyzed. Micronuclei with undamaged (left; negative γH2A.X signal) and damaged (right; positive γH2A.X signal) DNA were observed in all analyzed embryos. Zoomed images of micronuclei are shown on the right of each image. Scale bar is 10 μm. **c,** TUNEL assay in apoptotic *X. tropicalis* and $t_e \times l_s$ hybrid embryos. *X. tropicalis* (left), *X. tropicalis* treated with cycloheximide (middle left) or

hydroxyurea (middle right) as indicated, and $t_e \times l_s$ hybrid (right) embryos were prepared for TUNEL assay 5 hpf (equivalent stage 9; top), 7 hpf (equivalent stage 10; middle) and 9.5 hpf (equivalent stage 10.5; bottom). Identical results were obtained over 3 different experiments. Representative images are shown and were taken under identical conditions.
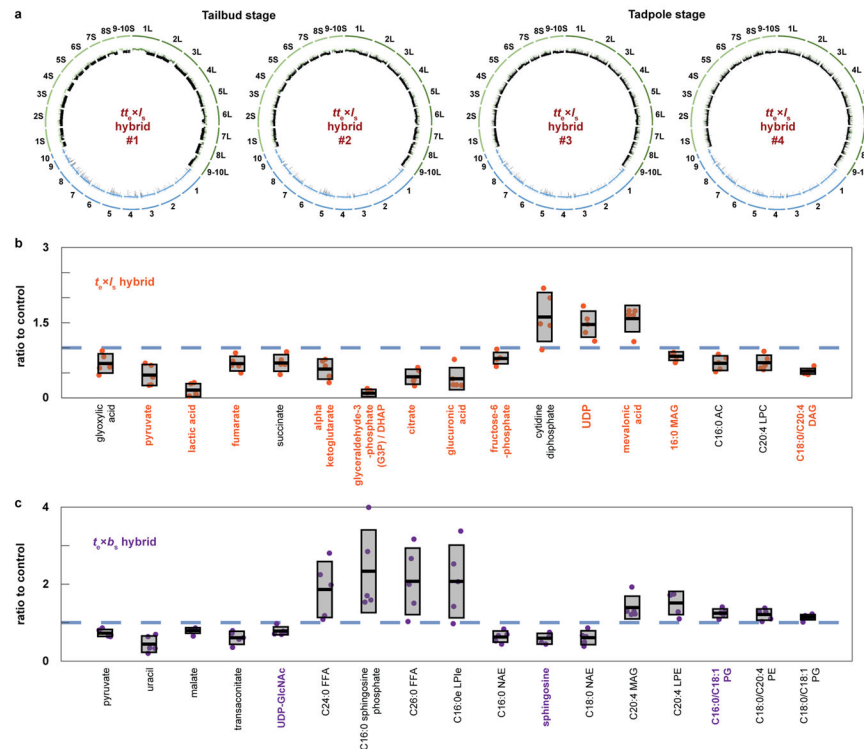
Extended Data Figure 3. Whole genome sequencing of $tt_e \times l_s$ rescued embryos and metabolomic profiling of $t_e \times l_s$ and $t_e \times b_s$ hybrid embryos

a, The genomes of 4 $tt_e \times l_s$ rescued embryos were sequenced, aligned, and normalized to the genomes of *X. tropicalis* (blue) and *X. laevis* (green) for which sub-genomes S and L were distinguished (S in light green and L in dark green). Underrepresented regions of the genomes are color-coded in black. The $tt_e \times l_s$ embryo genomes 1–2 were prepared from tailbuds, and 3–4 from tadpoles. **b,** Metabolites differentially represented between $t_e \times l_s$ hybrid and *X. tropicalis* embryos 7 h post fertilization. Among the 179 metabolites detected, 17 were significantly altered in $t_e \times l_s$ hybrid embryos (p < 0.05; two-tailed homoscedastic t-test; individual p-values are provided in Figure 3c source data) and are shown as a ratio to the *X. tropicalis* control (blue dashed line). Levels were obtained from 5 samples from 3 independent fertilizations each. Values for the $t_e \times l_s$ hybrid are plotted in orange. The averages are shown as thick lines and the gray boxes correspond to 1 standard deviation. 95% confidence intervals are, from left to right, 0.69±0.24, 0.46±0.26, 0.16±0.16, 0.68±0.18, 0.70±0.21, 0.58±0.25, 0.10±0.09, 0.42±0.19, 0.38±0.27, 0.79±0.15, 1.61±0.61, 1.47±0.33, 1.58±0.33, 0.83±0.11, 0.71±0.18, 0.70±0.19, and 0.53±0.08. Metabolites with p values below the penalized Bonferroni corrected threshold (n = 12) are labeled in orange. **c,** Metabolites differentially represented between $t_e \times b_s$ hybrid and *X. tropicalis* embryos 7 h post fertilization. Among the 241 metabolites detected, 17 were significantly altered in $t_e \times b_s$ hybrid embryos (p < 0.05; two-tailed homoscedastic t-test; individual p-values are provided

in Figure 4g source data) and are shown as a ratio to the *X. tropicalis* control (blue dashed line). Levels were obtained from 5 samples from 3 independent fertilizations, each. Values for the $t_e \times b_s$ hybrid are plotted in purple. The averages are shown as thick lines and the gray boxes correspond to 1 standard deviation. 95% confidence intervals are, from left to right, 0.73±0.12, 0.44±0.26, 0.80±0.10, 0.61±0.21, 0.78±0.14, 1.86±0.9, 2.33±1.33, 2.07±1.07, 2.07±1.17, 0.63±0.19, 0.59±0.16 0.61±0.22, 1.39±0.37, 1.51±0.38, 1.24±0.14, 1.21±0.18, and 1.14±0.10. Metabolites with p values below the penalized Bonferroni corrected threshold (n = 3) are labeled in purple.
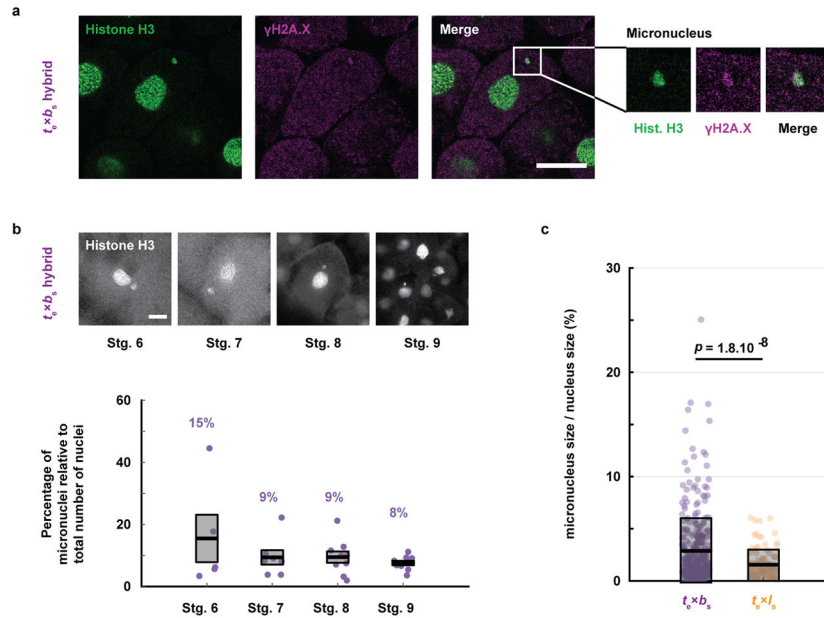
Extended Data Figure 4. Characterization of micronuclei in $t_e \times b_s$ hybrid embryos
a, DNA damage in $t_e \times b_s$ hybrid embryo micronuclei. Whole mount embryo immunofluorescence was performed in $t_e \times b_s$ hybrid embryos using anti-histone H3 (left) and anti-γH2A.X (middle) antibodies, corresponding channels are shown in green and magenta, respectively. The merged image is shown on the right. 34 micronuclei within 8 different embryos were analyzed. Micronuclei with damaged DNA were observed in all analyzed embryos. Zoomed images of micronuclei are shown on the right in the same left-to-right order. Scale bar is 20 μm. **b,** Micronuclei in $t_e \times b_s$ hybrid embryos at various developmental stages (top). Whole mount embryo immunofluorescence was performed in $t_e \times b_s$ hybrid embryos using anti-histone H3 antibody at stages 6, 7, 8 and 9. Scale bar is 20 μm. Quantification of micronuclei in $t_e \times b_s$ hybrid embryos (bottom). The percentage of micronuclei was calculated as the number of micronuclei in the imaged portion of the embryo divided by the total number of nuclei in the same imaged portion. The average percentage for multiple embryos at stage 6 (n = 5 $t_e \times b_s$ hybrid embryos (individual dots) with a total of 125 nuclei), stage 7 (n = 7/153), stage 8 (n = 9/731) and stage 9 (n = 10/2691) is shown as a thick line. Gray boxes correspond to 1 standard error of the mean. Control *X. tropicalis* embryos from the same mothers were analyzed but no micronuclei were observed at any stages. **c,** Micronuclei size in $t_e \times b_s$ and $t_e \times l_s$ hybrids. Size is plotted as the ratio between the volumes of the micronucleus and its corresponding nucleus. Each dot represents

an individual data point (n = 329 micronuclei from 36 $t_e \times b_s$ embryos shown in purple and n = 100 from 17 $t_e \times l_s$ embryos shown in orange, from 4 independent experiments). The thick black line indicates the average and the grey box corresponds to 1 standard deviation. 95% confidence intervals are 2.9±0.36% for $t_e \times b_s$ and 1.6±0.28% for $t_e \times l_s$ embryos. Statistical significance was shown using a two-tailed heteroscedastic t-test.

Extended Data Table 1
Embryonic development in *Xenopus* haploids and cybrids generated from *X. tropicalis* irradiated eggs

n indicates the number of different male-female combinations from which results were compiled. Unfertilized eggs and embryos that showed an abnormal or incomplete first cleavage were excluded from this analysis (†). Fertilization efficiency of irradiated *X. tropicalis* eggs with *X. laevis* sperm was very low (~4%) (‡).

Embryo	Normal Stage 2†(n)	Regular Stage 9 (%)	Died between 9–13 (%)	Exogastrulae	Normal tailbuds	Abnormal tailbuds	Tadpoles	
							Stunted (%)	Normal (%)
$[t_e] \times t_s$	402 (5)	402(100)	6(1)	131 (33)	209 (52)	56 (14)	191 (48)	18(4)
$[t_e] \times l_s^{‡}$	25(7)	25(100)	25(100)	0(0)	0(0)	0(0)	0(0)	0(0)

Extended Data Table 2
Effects of drug treatments on $t_e \times t_s$ embryos

X. tropicalis embryos were treated with different drugs at different stages. Phenotypes of effects are listed. When unspecified, apoptosis or lysis initiated at random locations in the embryo.

Drug	Inhibition	Time of addition	Concentration	Phenotype	Product details
Cycloheximide	Protein synthesis	stage 6.5	0.1 mg/ml	Cell cycle arrest at stage 7 followed by apoptosis	C7698 (Sigma-Aldrich)
Hydroxyurea	DNA replication	stage 3	30 mM	Apoptosis at late stage 8	AC151680050 (Thermo Fisher Sc.)
Triptolide	Transcription	stage 2	25 µM	Cell lysis at stage 9	T3652 (Sigma-Aldrich)
Olygomycin	ATP Synthase	stage 2	40 µM	Cell cycle arrest at stage 9	75351 (Sigma-Aldrich)
AP-III-a4	Enolase (including non-glycolytic functions)	stage 2	30 µM	Arrest at stage 7 and followed by cell lysis	19933 (Cayman Chemical)
Iodoacetic acid	Glyceraldehyde-3-P dehydrogenase	stage 2	50 mM	Cell lysis at stage 9	14386 (Sigma-Aldrich)
CP-91,149	Glycogen phosphorylase	stage 2	270 µM	Cell death at stage 9 from the	PZ0104 (Sigma-Aldrich)

Drug	Inhibition	Time of addition	Concentration	Phenotype	Product details
				vegetal side	

Extended Data Table 3
Sub genome distribution of lost vs. retained DNA in $t_e \times l_s$, $tt_e \times l_s$, and $t_e \times b_s$ hybrids

Percentage of lost and remaining DNA for each sub genome is shown for all hybrid genomes sequenced. Sub genomes are color-coded as in Figures 2c and 4e.

$t_e \times l_s$ hybrid

Sub genome	Total (bp)	Lost (bp)	Remaining (bp)	Lost (%)	Remaining (%)
X laevis L	1368982762	237294229	1131688533	17.33	82.67
X. laevis S	1139955720	11850000	1128105720	1.04	98.96
X. tropicalis	1272999256	3452000	1269547256	0.27	99.73

$tt_e \times l_s$ hybrid #1

Sub genome	Total (bp)	Lost (bp)	Remaining (bp)	Lost (%)	Remaining (%)
X. laevis L	1368982762	1084660643	284322119	79.23	20.77
X. laevis S	1139955720	946048452	193907268	82.99	17.01
X. tropicalis	1272999256	5686000	1267313256	0.45	99.55

$tt_e \times l_s$ hybrid #2

Sub genome	Total (bp)	Lost (bp)	Remaining (bp)	Lost (%)	Remaining (%)
X. laevis L	1368982762	1259268028	109714734	91.99	8.01
X. laevis S	1139955720	1003939197	136016523	88.07	11.93
X tropicalis	1272999256	2964000	1270035256	0.23	99.77

$tt_e \times l_s$ hybrid #3

Sub genome	Total (bp)	Lost (bp)	Remaining (bp)	Lost (%)	Remaining (%)
X. laevis L	1368982762	1360054762	8928000	99.35	0.65
X laevis S	1139955720	1131571720	8384000	99.26	0.74
X tropicalis	1272999256	3728000	1269271256	0.29	99.71

$tt_e \times l_s$ hybrid #4

Sub genome	Total (bp)	Lost (bp)	Remaining (bp)	Lost (%)	Remaining (%)
X. laevis L	1368982762	1361764762	7218000	99.47	0.53
X laevis S	1139955720	1134337720	5618000	99.51	0.49
X. tropicalis	1272999256	3240000	1269759256	0.25	99.75

$t_e \times b_s$ hybrid

Sub genome	Total (bp)	Lost (bp)	Remaining (bp)	Lost (%)	Remaining (%)
X. borealis L	1428994000	108866000	1320128000	7.62%	92.38%
X. borealis S	1201786000	30804000	1170982000	2.56%	97.44%
X tropicalis	1273010000	11592000	1261418000	0.91%	99.09%

Extended Data Table 4

Overrepresentation test of all or metabolism-only 3L and 4L lost genes

PANTHER software (http://pantherdb.org/) was used to perform a statistical overrepresentation test on all (top table) or metabolism-only (bottom table) lost genes from chromosomes 3L and 4L. Only overrepresented processes are shown in the top table (*). Only the top 5 processes based on fold enrichment are shown in the bottom table (†).

3L and 4L lost genes overrepresentation test

Analysis Type	PANTHER Overrepresentation Test (release 20170413)
Annotation Version and Release Date	PANTHER version 11.1 Released 2016-10-24
Analyzed List	Client Text Box Input (Xenopus tropicalis)
Reference List	Xenopus tropicalis (all genes in database)
Bonferroni correction	TRUE

PANTHER GO-Slim Biological Process*	Xenopus tropicalis - REFLIST (18238)	Client Text Box Input (843)	Client Text Box Input (expected)	Client Text Box Input (fold Enrichment)	Client Text Box Input (P-value)	95% Confidence Interval (binomial test)
biosynthetic process (GO:0009058)	1295	141	100.05	1.41	8.01E-03	[123.4, ∞]
nitrogen compound metabolic process (GO:0006807)	1738	179	134.27	1.33	1.40E-02	[159.6, ∞]
metabolic process (GO:0008152)	6036	546	466.32	1.17	1.13E-03	[522.4, ∞]

3L and 4L lost metabolism genes overrepresentation test

Analysis Type	PANTHER Overrepresentation Test (release 20170413)
Annotation Version and Release Date	PANTHER version 11.1 Released 2016-10-24
Analyzed List	Client Text Box Input (Xenopus tropicalis)
Reference List	Xenopus tropicalis (all genes in database)
Bonferroni correction	TRUE

PANTHER GO-Slim Biological Process†	Xenopus tropicalis - REFLIST (18238)	Client Text Box Input (843)	Client Text Box Input (expected)	Client Text Box Input (fold Enrichment)	Client Text Box Input (P-value)	95% Confidence Interval (binomial test)
glycolysis (GO:0006096)	26	6	0.78	7.71	3.71E-02	[2.6, ∞]
rRNA metabolic process (GO:0016072)	104	15	3.11	4.82	2.22E-04	[9.3, ∞]
DNA replication (GO: 0006260)	114	16	3.41	4.69	1.38E-04	[10.1, ∞]
tRNA metabolic process (GO:0006399)	104	14	3.11	4.5	1.11E-03	[8.5, ∞]
generation of precursor metabolites and energy (GO:0006091)	185	24	5.54	4.33	9.87E-07	[16.6, ∞]

Supplementary Material

Refer to Web version on PubMed Central for supplementary material.

Acknowledgments

References

1. Seehausen O, et al. Genomics and the origin of species. Nat Rev Genet. 2014; 15:176–192. [PubMed: 24535286]

2. Presgraves DC. The molecular evolutionary basis of species formation. Nat Rev Genet. 2010; 11:175–180. [PubMed: 20051985]

3. Session AM, et al. Genome evolution in the allotetraploid frog Xenopus laevis. Nature. 2016; 538:1–15.

4. Brown KS, et al. Xenopus tropicalis egg extracts provide insight into scaling of the mitotic spindle. J Cell Biol. 2007; 176:765–70. [PubMed: 17339377]

5. Hirsch N, Zimmerman LB, Grainger RM. Xenopus, the next generation: X. tropicalis genetics and genomics. Dev Dyn. 2002; 225:422–33. [PubMed: 12454920]

6. Yanai I, Peshkin L, Jorgensen P, Kirschner MW. Mapping gene expression in two Xenopus species: evolutionary constraints and developmental flexibility. Dev Cell. 2011; 20:483–96. [PubMed: 21497761]

7. Bürki E. The expression of creatine kinase isozymes in Xenopus tropicalis, Xenopus laevis laevis, and their viable hybrid. Biochem Genet. 1985; 23:73–88. [PubMed: 3994660]

8. Narbonne P, Simpson DE, Gurdon JB. Deficient induction response in a Xenopus nucleocytoplasmic hybrid. PLoS Biol. 2011; 9:e1001197. [PubMed: 22131902]

9. Hamilton L. Androgenic haploids of a toad, Xenopus laevis. Nature. 1957; 179:159. [PubMed: 13400130]

10. Goda T, et al. Genetic screens for mutations affecting development of Xenopus tropicalis. PLoS Genet. 2006; 2:e91. [PubMed: 16789825]

11. Wühr M, et al. Evidence for an upper limit to mitotic spindle length. Curr Biol. 2008; 18:1256–61. [PubMed: 18718761]

12. Cheeseman IM. The Kinetochore. Cold Spring Harb Perspect Biol. 2014; 6:77–105.

13. Fujiwara, a, Abe, S., Yamaha, E., Yamazaki, F., Yoshida, MC. Uniparental chromosome elimination in the early embryogenesis of the inviable salmonid hybrids between masu salmon female and rainbow trout male. Chromosoma. 1997; 106:44–52. [PubMed: 9169586]

14. Sakai C, et al. Chromosome elimination in the interspecific hybrid medaka between Oryzias latipes and O. hubbsi. Chromosome Res. 2007; 15:697–709. [PubMed: 17603754]

15. Ferree PM, Barbash Da. Species-Specific Heterochromatin Prevents Mitotic Chromosome Segregation to Cause Hybrid Lethality in Drosophila. PLoS Biol. 2009; 7:e1000234. [PubMed: 19859525]

16. Kalitsis P, Choo KHA. The evolutionary life cycle of the resilient centromere. Chromosoma. 2012; 121:327–40. [PubMed: 22527114]

17. Crasta K, et al. DNA breaks and chromosome pulverization from errors in mitosis. Nature. 2012; 482:53–8. [PubMed: 22258507]

18. Hatch EM, Fischer AH, Deerinck TJ, Hetzer MW. Catastrophic nuclear envelope collapse in cancer cell micronuclei. Cell. 2013; 154:47–60. [PubMed: 23827674]

19. Terradas M, Martín M, Tusell L, Genescà A. DNA lesions sequestered in micronuclei induce a local defective-damage response. DNA Repair (Amst). 2009; 8:1225–34. [PubMed: 19683478]

20. Hensey C, Gautier J. A developmental timer that regulates apoptosis at the onset of gastrulation. Mech Dev. 1997; 69:183–195. [PubMed: 9486540]

21. Vastag L, et al. Remodeling of the metabolome during early frog development. PLoS One. 2011; 6:e16881. [PubMed: 21347444]

22. Ma H, et al. Incompatibility between Nuclear and Mitochondrial Genomes Contributes to an Interspecies Reproductive Barrier. Cell Metab. 2016; 24:283–294. [PubMed: 27425585]

23. Lee HY, et al. Incompatibility of Nuclear and Mitochondrial Genomes Causes Hybrid Sterility between Two Yeast Species. Cell. 2008; 135:1065–1073. [PubMed: 19070577]

24. Mi H, Poudel S, Muruganujan A, Casagrande JT, Thomas PD. PANTHER version 10: Expanded protein families and functions, and analysis tools. Nucleic Acids Res. 2016; 44:D336–D342. [PubMed: 26578592]

25. Schmid M, Steinlein C. Chromosome Banding in Amphibia. XXXII. the Genus Xenopus (Anura, Pipidae). Cytogenet Genome Res. 2015; 145:201–217. [PubMed: 26112092]

26. Nieuwkoop, PD., Faber, J. Normal table of Xenopus laevis (Daudin). Garland Publishing; 1994.

27. Schindelin J, et al. Fiji: an open-source platform for biological-image analysis. Nature Methods. 2012; 9:676–682. [PubMed: 22743772]

28. Lee C, Kieserman E, Gray RS, Park TJ, Wallingford J. Whole-mount fluorescence immunocytochemistry on Xenopus embryos. CSH Protoc. 2008; 2008 pdb.prot4957.

29. Levy DL, Heald R. Nuclear size is regulated by importin α and Ntf2 in Xenopus. Cell. 2010; 143:288–98. [PubMed: 20946986]

30. Maresca TJ, Heald R. Methods for studying spindle assembly and chromosome condensation in Xenopus egg extracts. Methods Mol Biol. 2006; 322:459–74. [PubMed: 16739744]

31. Murray, aW. Cell cycle extracts. Methods Cell Biol. 1991; 36:581–605. [PubMed: 1839804]

32. Hannak E, Heald R. Investigating mitotic spindle assembly and function in vitro using Xenopus laevis egg extracts. Nat Protoc. 2006; 1:2305–14. [PubMed: 17406472]

33. Edelstein AD, et al. Advanced methods of microscope control using μManager software. J Biol Methods. 2014; 1:10.

34. Robinson MD, McCarthy DJ, Smyth GK. edgeR: a Bioconductor package for differential expression analysis of digital gene expression data. Bioinformatics. 2010; 26:139–40. [PubMed: 19910308]

35. Ritchie ME, et al. limma powers differential expression analyses for RNA-sequencing and microarray studies. Nucleic Acids Res. 2015; 43:e47. [PubMed: 25605792]

36. Louie SM, et al. GSTP1 Is a Driver of Triple-Negative Breast Cancer Cell Metabolism and Pathogenicity. Cell Chem Biol. 2016; 23:567–78. [PubMed: 27185638]
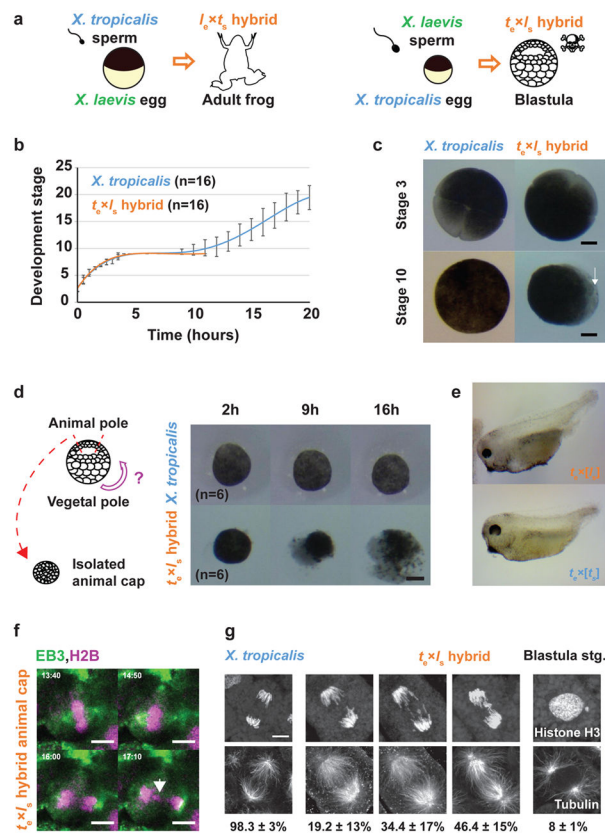
Figure 1. Role of the *X. laevis* genome in $t_e \times l_s$ hybrid embryo death

a, Schematic of *X. laevis* and *X. tropicalis* cross-fertilization outcomes. **b,** Developmental timing in *X. tropicalis* and $t_e \times l_s$ hybrid embryos. Average is plotted for each time point. Error bars show standard deviation. **c,** Representative images of *X. tropicalis* and $t_e \times l_s$ hybrid embryos at stages 3 and 10 from experiments in b (n = 16 *X. tropicalis* and n = 16 $t_e \times l_s$ hybrid embryos from 4 independent experiments). The arrow indicates vegetal cells where death initiates. **d,** Schematic of animal cap assay and images of at 2, 9 and 16 h after isolation. 6 animal caps were imaged and identical results were obtained in 3 different experiments. Scale bars in c and d, 200 μm. **e,** Images showing haploid phenotype following fertilization of *X. tropicalis* eggs with UV-irradiated sperm. Identical results were observed in n = 3 experiments. **f,** Time-lapse images of dividing cell in a $t_e \times l_s$ hybrid animal cap (Video 5). The arrow indicates a mis-segregated chromosome. Mis-segregated chromosomes were observed in n = 3 live $t_e \times l_s$ hybrid animal caps in 3 experiments. Time is in mm:ss. **g,** Immunofluorescence images showing chromosome bridges, mis-segregated chromosomes, and micronuclei throughout $t_e \times l_s$ hybrid embryos. Scale bars in f and g are 10 μm. Quantification of n = 81 *X. tropicalis* and n = 78 $t_e \times l_s$ hybrid anaphases in n = 17 and 16 embryos, respectively, from 4 datasets obtained from 3 experiments presented as averages ± 1 standard deviation, show a significant difference by Fisher 2 by 3 contingency test (p = 0). Quantification of micronuclei in $t_e \times l_s$ hybrid embryos is detailed in Extended Data Figure 1b.
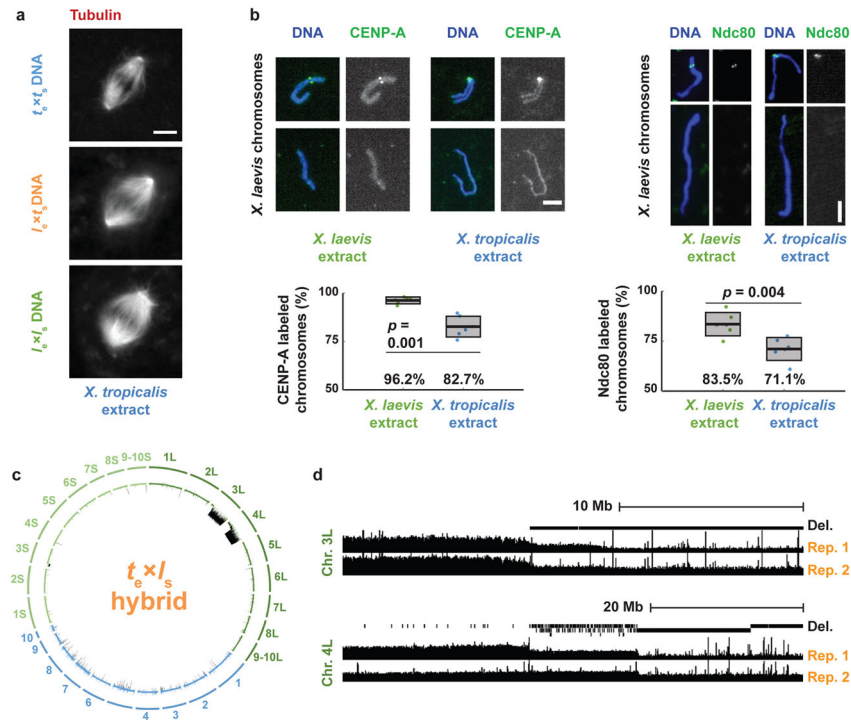
Figure 2. Compatibility of *X. laevis* chromosomes with *X. tropicalis* cytoplasm
a, Fluorescence images of spindles formed around *X. tropicalis*, $l_e \times t_s$ hybrid, and *X. laevis* chromosomes in *X. tropicalis* egg extract. Scale bar, 10 μm. Quantification for n = 147, 103, and 156 spindles quantified for *X. tropicalis*, $l_e \times t_s$ hybrids, and *X. laevis* embryo nuclei, respectively, from 3 different egg extracts, is presented in Extended Data Figure 1e. **b,** Fluorescence images of *X. laevis* chromosomes stained for CENP-A or Ndc80 following replication in *X. laevis* or *X. tropicalis* egg extract. CENP-A and Ndc80 labeling was quantified from 6 experiments (3 biological replicates in 2 technical replicates), a total of n = 1792 and n = 1959 chromosomes, respectively in *X. laevis* extract, and n = 2692 and n = 1930, respectively, in *X. tropicalis* extract. Scale bars, 5 μm. Box plots show the 6 experiment percentages as individual data points, their average as thick lines, and 1 standard deviation as gray boxes. 95% confidence intervals are 96.2±1.9% in *X. laevis* extract vs. 82.7±5.7% in *X. tropicalis* extract for CENP-A and 83.5±6.1% vs. 71.1±6.0% for Ndc80. P-values were determined by two-tailed heteroscedastic t-test. **c,** Circle plot of whole genome sequencing data for $t_e \times l_s$ hybrid embryos aligned and normalized to the genomes of *X. tropicalis* (blue) and *X. laevis* (green), with underrepresented genome regions in black. **d,** Expanded view of chromosome 3L and 4L breakpoints with deleted regions indicated in two biological replicates.
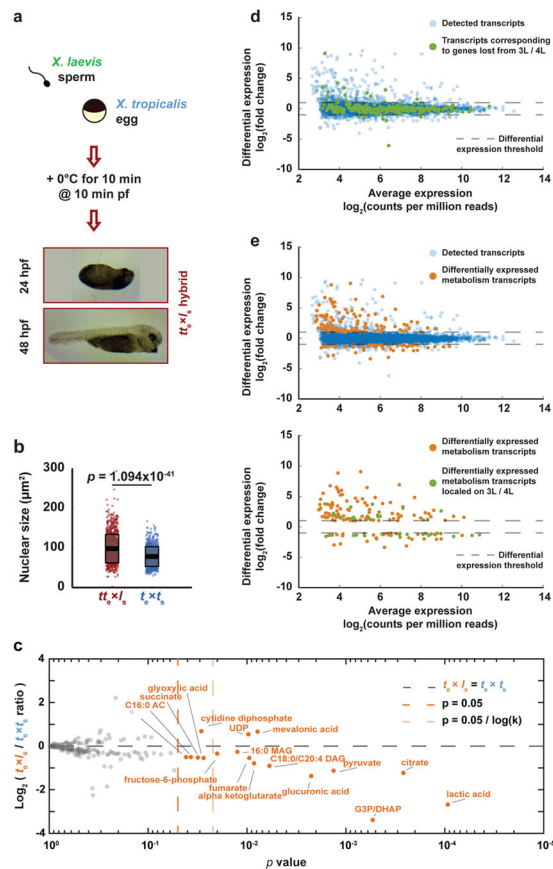
Figure 3. Gene expression and metabolic changes preceding $t_e \times l_s$ hybrid embryo death

a, Schematic of polar body suppression experiment and images of $tt_e \times l_s$ rescued embryos 24 h and 48 h post-fertilization (hpf). A total of 9 $tt_e \times l_s$ embryos were obtained in 4 different experiments. **b,** Box plot of nuclear sizes (n = 988 nuclei from 3 $tt_e \times l_s$ embryos and n = 777 from 3 *X. tropicalis* embryos at stage 21) showing the average area as thick lines and 1 standard deviation as gray boxes. 95% confidence intervals are 98.1±2.2 μm² for $tt_e \times l_s$ and 78.0±1.7 μm² for *X. tropicalis* embryos. P-values were determined by two-tailed heteroscedastic t-test. **c,** Levels of 179 metabolites in *X. tropicalis* and $t_e \times l_s$ hybrid embryos 7 hpf. Levels were obtained from 5 samples from 3 independent fertilizations, each averaged and plotted as Log₂ of the ratio with the control (see Methods). P-values were calculated using a two-tailed homoscedastic t-test. The average and 1 standard deviation for the differentially represented metabolites are shown, and 95% confidence intervals given in Extended Data Figure 3b. **d,** Differential gene expression between $t_e \times l_s$ and $t_e \times t_s$ (see Methods). All detected transcripts (n = 8379) are plotted in blue. Transcripts corresponding to genes lost from chromosomes 3L and 4L (n = 270) are plotted in green. **e,** Differential expression of metabolism genes between $t_e \times l_s$ and $t_e \times t_s$ (see Methods). Differentially expressed metabolism transcripts (n = 165) are plotted in orange, all detected transcripts (n = 8379) in blue (top), and differentially expressed metabolism transcripts located on chromosomes 3L and 4L (n = 35) in green (bottom).
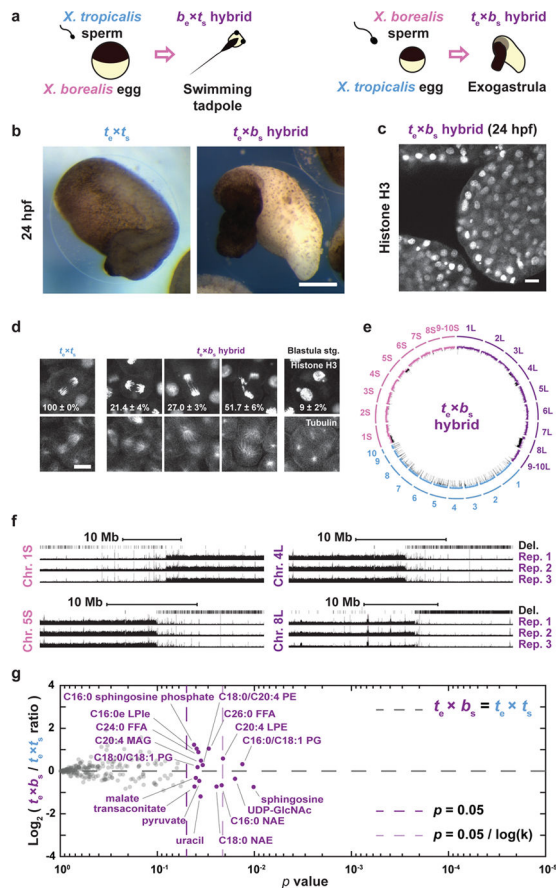
Figure 4. Chromosomal loss in exogastrulating $t_e \times b_s$ hybrid embryos

a, Schematic of *X. borealis* and *X. tropicalis* cross-fertilization outcomes. **b,** Representative images of $t_e \times t_s$ vs. $t_e \times b_s$ embryos at 24 hpf. This result was reproduced in 4 separate experiments. Scale bar, 200 μm. **c,** Immunofluorescence image of $t_e \times b_s$ hybrid embryo at 24 hpf showing nuclei and micronuclei. Similar defects at this stage were observed in 6 different embryos. **d,** Immunofluorescence images showing chromosome bridges, mis-segregating chromosomes, and micronuclei throughout $t_e \times l_s$ hybrid embryos. Scale bars, 20 μm. Quantification of n = 33 *X. tropicalis* and 63 $t_e \times b_s$ hybrid anaphases in n = 6 and 12 embryos, respectively, show a significant difference by Fisher 2 by 3 contingency test (p = 0). Quantification of micronuclei in $t_e \times b_s$ hybrid embryos is detailed in Extended Data Figure 4b. **e,** Circle plot of whole genome sequencing data for $t_e \times b_s$ hybrid embryos aligned and normalized to the genomes of *X. tropicalis* (blue) and *X. borealis* (purple). Underrepresented genome regions (black) represent 9.674% of chromosome 4L, 74.66% of 8L, 4.71% of 1S, and 14.4% of 5S. **f,** Expanded view of chromosome 1S, 5L, 4L and 8L breakpoints with deleted regions indicated in three biological replicates. **g,** Levels of 241 metabolites in *X. tropicalis* and $t_e \times b_s$ hybrid embryos 7 hpf (see Methods). Levels were obtained from 5 samples from 3 independent fertilizations, each, averaged and plotted as Log_2 of the ratio with the control (see Methods). P-values were calculated using a two-tailed homoscedastic t-test. The average and 1 standard deviation for the differentially represented metabolites are shown, and 95% confidence intervals given in Extended Data Figure 3c.

Note that few metabolites are altered significantly and are distinct from those altered in $t_e \times l_s$ hybrids (see Extended Data Figure 3b–c).